Critical Size of Silver Iodide Containing Glaciogenic Cloud Seeding Particles

Jie Chen[1, *], Carolin Rösch[1, #], Michael Rösch[1], Aleksei Shilin[2], Zamin A. Kanji[1, *]

[1] Institute for Atmospheric and Climate Science, ETH Zürich, Zurich, 8092, Switzerland
[2] Cloud Seeding Technologies, Burgenstrasse 22, Gaertringen, 71116, Germany
[#] Now at City of Zurich, Environment and Health Safety, Air Quality Division, Zurich Switzerland

[*] Corresponding authors:
Zamin A. Kanji zamin.kanji@env.ethz.ch and Jie Chen jie.chen@env.ethz.ch

Key points

- Silver iodide (AgI) containing aerosols generated under cloud-seeding relevant conditions exhibit a size-dependent ice-forming ability
- Non-AgI impurities produced from flare burning decrease the ice nucleation ability of particles smaller than 90 nm
- A new parameterization is presented to estimate the minimum mass concentration of AgI particles required to maximize glaciogenic seeding

Abstract

Cloud seeding is considered a practical but unproved method to enhance precipitation or suppress hail, due to the insufficient knowledge of ice formation and evolution after seeding clouds with ice nucleating particles. This study investigates the aerosol size effects on the ice nucleation of commercial silver iodide (AgI) containing flares under cloud-seeding conditions. The generated aerosol exhibited comparable ice nucleation ability (INA) to pure AgI particles in the size range of 200 and 400 nm. Non-AgI impurities reduced the INA of flare particles <90 nm, which is higher when compared to pure AgI (< 40 nm). The critical mass ice-active site density of the generated aerosols (*critical-*n_m) was derived based on our findings, indicating the minimum mass concentration of AgI particles required for efficient ice nucleation. The new parameterization to predict *critical-*n_m can serve as a reference to optimize the effectiveness of cloud-seeding materials for practical use.

Plain Language Summary

Ice-forming aerosol is commonly added to clouds, expecting precipitation enhancement via promotion of ice production. In this work, silver iodide (AgI) containing aerosol was generated from commercial cloud-seeding products under different wind speed conditions. Its ice-forming ability was studied at mixed-phase cloud temperatures. The lower size limit for effective ice-forming ability of the cloud-seeding particles (90 nm) is higher than that of pure AgI particles (40 nm). The non-AgI components produced by cloud-seeding products are hypothesized to decrease the ice-forming ability of smaller particles, as the mass fraction of ice-nucleating AgI particles decreases. To estimate the minimum concentration of ice-forming AgI particles required for efficient ice nucleation under cloud-seeding relevant conditions, we derived the critical ice-activated mass fraction of the generated aerosols. These findings provide valuable insights into the optimization of cloud-seeding practices for enhanced precipitation.

1 Introduction

Ice crystals are important constituents of cold clouds (temperature < 0 ^{o}C) because their number concentration and size largely regulate cloud microphysics [*Lamb*, 2003] and impact cloud radiative properties and precipitation formation [*Lohmann et al.*, 2016]. Ice formation in the atmosphere can be initiated by the homogeneous freezing of supercooled cloud droplets [*Koop et al.*, 2000] or via heterogeneous nucleation aided by ice-nucleating particles (INPs) [*Cantrell and Heymsfield*, 2005; *Fletcher*, 1970; *Kanji et al.*, 2017; *Murray et al.*, 2012]. The presence of INPs lowers the energy barrier for ice embryos to form and facilitates a phase change under conditions where the homogeneous freezing rate is too small. If cloud droplets are artificially perturbed by the addition of INPs, the cloud microphysical processes are expected to change. As such INPs are of specific interest in weather modification to enhance precipitation [*Rauber et al.*, 2019] or suppress hail [*Dessens et al.*, 2016] by promoting ice production under appropriate meteorological and cloud water conditions. Ambiguous conclusions on the efficiency of previous cloud-seeding projects [*French et al.*, 2018; *Friedrich et al.*, 2020; *Kerr*, 1982; *Manton and Warren*, 2011; *Pokharel et al.*, 2017; *Rauber et al.*, 2019; *Silverman*, 2010] indicate that large uncertainties still exist in how INPs work under different meteorological conditions to change cloud properties and produce precipitation. For glaciogenic cloud seeding to work, the first step is to identify the ice nucleation ability (INA) of commercially available cloud-seeding aerosols.

Silver iodide (AgI) containing particles are widely used in cloud-seeding programs [*French et al.*, 2018; *Friedrich et al.*, 2020; *Kerr*, 1982; *Manton and Warren*, 2011; *Pokharel and Geerts*, 2016; *Pokharel et al.*, 2017; *Rauber et al.*, 2019; *Silverman*, 2010] due to its strong INA in the heterogeneous freezing regime [*DeMott*, 1995; *Marcolli et al.*, 2016; *Nagare et al.*, 2016; *Vonnegut*, 1947; *Vonnegut*, 1949]. Laboratory experiments have been conducted to investigate the ice nucleation mechanism of pure AgI particles. The reason for its effect on ice nucleation is imputed to its surface properties, including lattice matches with ice [*Davis et al.*, 1975; *Palanisamy et al.*, 1986], surface defects [*Shevkunov*, 2005; 2008], and surface charges [*Edwards et al.*, 1962] which are important for the ice nucleation of AgI particles at or above water saturation [*DeMott*, 1995; *DeMott et al.*, 1983; *Edwards et al.*, 1962; *Marcolli et al.*, 2016].

The INAs of AgI-containing aerosols generated through different materials and methods were investigated and showed distinct results [*Davis et al.*, 1975; *DeMott et al.*, 1983; *Edwards et al.*, 1962; *Marcolli et al.*, 2016]. The varied INAs are likely linked to the different physicochemical properties of the produced aerosols. AgI particles have shown modified INAs after mixing with other chemical components [*Davis et al.*, 1975; *DeMott et al.*, 1983], implying the importance of the chemical composition of AgI-containing aerosols in altering their INAs. Particle size is another crucial characteristic affecting the INA of AgI particles. Larger AgI particles have a higher probability of hosting an ice active site on the surface and therefore nucleate ice more effectively compared to smaller particles at identical temperature and relative humidity conditions [*DeMott*, 1995; *Edwards et al.*, 1962; *Marcolli et al.*, 2016]. The INA of AgI particles decreased significantly if sizes were < 40 nm, attributed to the partial dissolution of AgI particles in the cloud droplet [*Marcolli et al.*, 2016].

In realistic cloud-seeding operations, the chemical composition and size distribution of cloud-seeding aerosol are determined by the composition of the seeding materials and the meteorological conditions where the seeding is conducted. Commercial cloud-seeding products

contain non-AgI components that enable activation into cloud droplets prior to freezing under cloud-relevant conditions. These components have the potential to modify the chemical composition of cloud-seeding aerosol during its formation, although their exact impact on the INA of AgI particles remains unknown. The size distribution of the cloud-seeding aerosol is modulated by the encountered wind speeds, potentially playing a role in determining its INA. Nevertheless, the size distribution of cloud-seeding aerosols under varying wind speed conditions and the associated INAs have not been investigated so far.

The above-mentioned results underscore the importance of the chemical nature and particle size in determining the INA of cloud-seeding aerosol in realistic cloud-seeding operations, which is less investigated and poorly understood. In this work, the INAs of size-resolved commercially available cloud-seeding aerosols are tested under mixed-phase cloud temperature and relative humidity conditions. The AgI-containing aerosol was produced pyrotechnically from flares used in hail prevention programs in Switzerland under different wind speed conditions to test the effect of wind speed on the particle size distribution to mimic when flares are mounted on aircraft wings.

2 Methodology

The schematic of the experimental setup to generate the cloud-seeding aerosol, measure its size distribution and INA in the temperature range of 243 K to 267 K in the immersion freezing mode is shown in Figure S1. More descriptions are detailed in the following sections.

2.1 Generation of cloud-seeding aerosols

The AgI-containing aerosols were generated by igniting burn-in-place flares. The flare is a smaller and lower mass customized version of the burn-in-place ZEUS flares provided by Cloud Seeding Technologies for mounting on aircraft. The flares are composed of AgI (11.8%), iodine-containing compounds (15.3%) and other materials (such as ammonium perchlorate, catalysts, and fuel binder). The exact composition cannot be disclosed due to proprietary reasons. In each experiment, the investigated flare (7 mm in diameter) was fitted into the flare holder and ignited electronically in a customized fireproof burning chamber (BUC, Fig. S2). The design of BUC is detailed in the supporting information (SI) (Fig. S2, Text S1). Note that the unique design of the 3D-printed flare holder creates high wind speed conditions around flares (~25 m s^{-1}), which is expected to be an important factor in controlling the generated size distribution of particles. The generated aerosol was directed to a mixing tank after exhausting the first 20 seconds of burning (with a total burning time of approximately 90 seconds), after the burning stabilized. The mixing tank allows continued suspension of aerosol over a longer time for subsequent measurements of particle mass, size and ice nucleation by different instruments. Two different mixing tanks were used to study particles of different sizes. The small mixing tank with a volume of 0.12 m^3 (shown in Fig. S3) was used for experiments with particles of 200 and 400 nm sizes. A large stainless-steel aerosol tank with a volume of 2.7 m^3 [*Kanji et al.*, 2013], was used for a slower coagulation rate of particles so as to be able to select particles of smaller size. The total filling time was 3 seconds for the small tank and 10 seconds for the large tank, respectively, which was chosen to reduce coagulation of particles. Both tanks were run with overpressure valves to avoid overpressure during the filling process. Particle settling was reduced by running mixing fans mounted at the bottom of the two tanks. Nitrogen was continuously injected into the mixing tank to compensate for the air volume which was sampled by downstream particle detection instruments and the ice nucleation chamber.

2.2 Size selection and mass measurement of particles

The size distribution of the polydisperse aerosol particles was detected by a differential mobility particle spectrometer (DMPS) connected downstream of the tanks (see Text S2 for working details). The DMPS selected the monodisperse aerosol of one size (D_p) and the total number concentration of the selected particles ($N_{total\ particles}$) was measured by a Condensation Particle Counter (TSI Inc., CPC 3772), with a flow rate of 1 L min^{-1} (Fig. S1). The monodisperse aerosol was sampled by the ice nucleation chamber (Fig. S1). Occasionally, a centrifugal particle mass analyzer (CPMA, 1st generation, Cambustion Ltd.) with a flow rate of 1 L min^{-1} was connected to the monodisperse aerosol flow to measure the single-particle mass (see Text S3 for working details).

2.3 Ice nucleation measurements under mixed-phase cloud conditions

The INA of the cloud-seeding aerosol was measured by the combination of an immersion mode cooling chamber (IMCA) [*Lüönd et al.*, 2010] and the Zürich ice nucleation chamber (ZINC) [*Stetzer et al.*, 2008]. The IMCA-ZINC system has been used previously to investigate the immersion freezing of cloud droplets [*Lüönd et al.*, 2010; *Welti et al.*, 2019; *Welti et al.*, 2012]. Monodisperse aerosol was dried and sampled into IMCA with a relative humidity of ~120% with respect to water (RH_w). The high RH_w was caused by the temperature gradient (25 K) between the warm and cold walls of IMCA and needed to generate cloud droplet sizes in the short residence times (~10 seconds) [*Welti et al.*, 2012]. The two vertically placed walls are lined with wetted filter papers, whose temperatures are controlled by two recirculating thermostats (Lauda, RP290). Particles activate and grow into cloud droplets in IMCA and are then passed into the lower part of the IMCA where the temperature transitions to that of ZINC. By passing through the lower part of IMCA the cloud droplet temperature also transitions to 273 K before entering ZINC [*Stetzer et al.*, 2008; *Welti et al.*, 2012]. The activated droplets grow to approximately 18~20 μm in diameter when passing through the IMCA [*Welti et al.*, 2012].

ZINC is also a vertically oriented parallel plate chamber with ice-coated inner walls. The walls of ZINC are cooled to different temperatures to create a RH_w of 101 %. The freezing fraction of droplets can be detected at the temperature range of 233 K to 270 K for a fixed humidity in this case. The residence time of particles in ZINC is ~10 seconds. The total flow rate within the IMCA-ZINC system was kept at 10 L min^{-1} by an external pump (9 L min^{-1} of particle-free sheath air and 1 L min^{-1} of aerosol flow). The number concentration of particles (ice crystals and water droplets) was detected in situ by the Ice Optical Depolarization detector (IODE) (described in *Nicolet et al.* [2010]) mounted close to the exit of ZINC (Fig. S1). IODE differentiates ice crystals and cloud droplets by depolarizing polarised light in the case of aspherical ice crystals. The frozen fraction (FF) of droplets is calculated based on the number concentration of ice crystals ($N_{ice\ crystals}$) and droplets ($N_{droplets}$) at the operational temperature conditions, as indicated by Equation (1):

$$FF = \frac{N_{ice\ crystals}}{N_{ice\ crystals} + N_{droplets}} \quad (1)$$

A higher FF represents higher INA of the tested particles.

The number concentrations of particles (0.5~25 μm) were also detected by an optical particle counter (OPC, Lighthouse Remote 5104) at the outlet of ZINC (Fig. S1). An

evaporation section with RH_i =100% was connected to the lower part of the ZINC chamber downstream of IODE (Fig. S1), forcing cloud droplets to evaporate before counting by the OPC. Only particles that have sizes larger than 1.5 μm were defined as ice crystals. This threshold size was the maximum size that droplets can reach at a temperature slightly above homogeneous freezing (~-34 ^{o}C) and after shrinking in the evaporation section, determined by measuring the phase transition of dilute ammonium nitrate droplets depending on temperatures. The activated fraction (AF) of aerosols was calculated by the ratio of the number concentration of ice crystals ($N_{ice\ crystals}$) determined by OPC and the initial total particles ($N_{total\ particles}$) measured by CPC:

$$AF = \frac{N_{ice\ crystals}}{N_{total\ particles}} \tag{2}$$

The active site density per unit of mass (n_m) can be estimated based on AF and the mass for a single particle measured by CPMA (*M*, *Hiranuma et al.* [2015]) or calculated by the particle diameter (D_p) and the particle density (ρ) by assuming a spherical particle shape ($M = \frac{\pi \rho {D_p}^3}{6}$) in the case of pure AgI particles.

$$n_m\,(T) = \frac{-\ln\,(1 - AF)}{M} \tag{3}$$

Similarly, the active site density per unit of particle surface (n_s) can be estimated based on AF and the surface area ($S = \pi {D_p}^2$) of spherical particles (Equation (4)).

$$n_s\,(T) = \frac{-\ln\,(1 - AF)}{S} \tag{4}$$

The performance of the IMCA-ZINC system was tested and validated before being used (see more details in Text S4 and Fig. S4).

3 Results and Discussions

3.1 Size distribution of aerosols at different wind speeds

The sizes of the generated particles vary with the experienced wind speed in real seeding flights. Particle size distributions of the generated aerosols as a function of wind speed (1~70 m s^{-1}) was investigated as a separate experiment using a wind tunnel (Table S1). According to Table S1, particles of smaller size were produced under higher wind speed conditions. Additionally, it was shown that the size of the customized flare impacted the particle size distribution in a way that smaller particles were created with reduced flare diameters. The original commercial flare has a diameter of 24 mm and is usually operated at a wind speed of 70 m s^{-1} or even higher. The modal particle size generated under this condition is 52 nm. To be as close to the particle size that in the real seeding conditions, the customized flare with a diameter of 7 mm (used in the present study) should be ignited at a wind speed of 30 m s^{-1} to obtain a similar mode size (52 nm, bold numbers in Table S1). Such a high wind speed condition could not be reached within the burning chamber under our laboratory conditions. The maximum wind speed of 25 m s^{-1} surrounding the flare was achieved in the end which profits from the unique design of the flare holder.

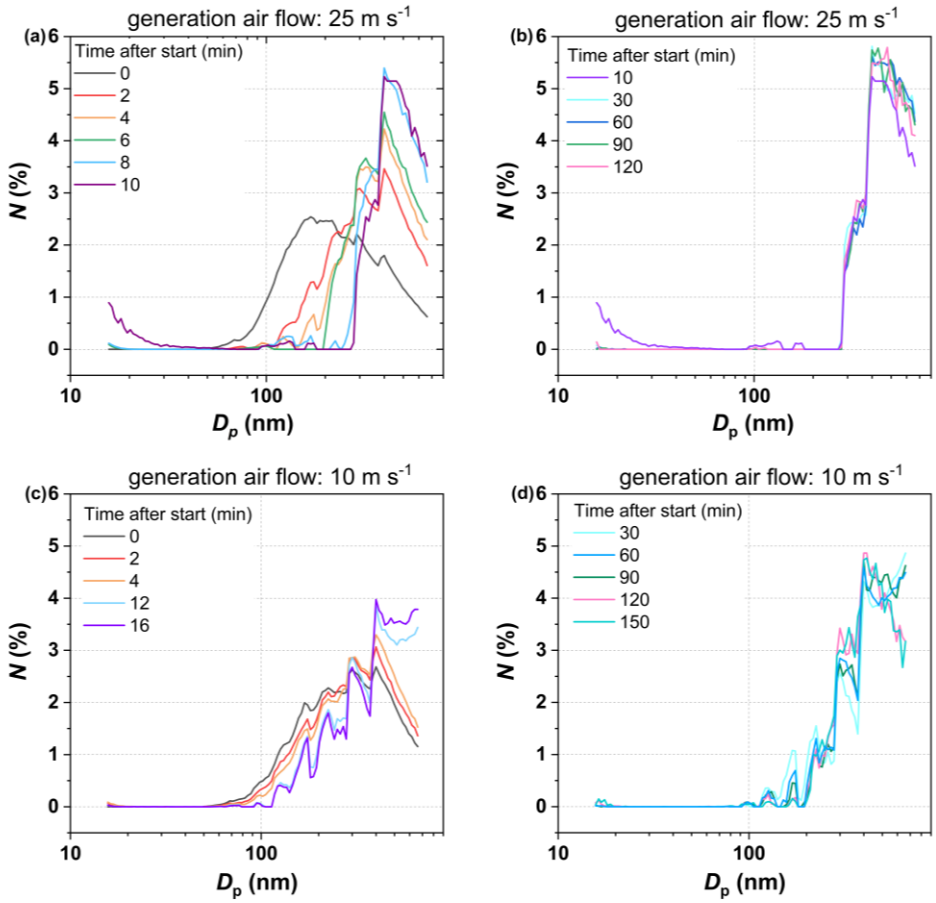

Figure 1. The temporal evolution of the number fraction (N(%)) of particles with different sizes (D_p) measured at wind speeds of 25 m s^{-1} (panels a and b) and 10 m s^{-1} (panels c and d). Data for the first ~16 minutes (panels a and c) and up to 150 minutes after the start (panels b and d) are shown.

The temporal evolution of particle size distribution generated at a wind speed of 10 and 25 m s^{-1} was monitored by the DMPS system and can be compared (Fig. 1). In general, the sizes of the generated particles ranged from 60 nm to 700 nm and changed rapidly within the first 10 minutes after tank filling (Figs. 1a and 1c). Thereafter, the particle size distribution shifted to larger sizes and stabilized for both applied wind speeds. The mode size reaches 400 ~ 500 nm with a few particles <100 nm. A narrower particle size distribution was observed at a wind speed of 25 m s^{-1} after being stable (300 ~ 700 nm, Fig. 1b and Fig. S5) compared to that at a wind speed of 10 m s^{-1} (100 ~ 700 nm, Fig. 1d and Fig. S5). The total number concentration of the particles decreased over time (Fig. S6). This is due to the experimental design which included a discrete fill period for the tank. Initially, particle coagulation plays a role in a shift of the size distribution to larger sizes and reducing the total particle concentration. After 10-20 mins, continued dilution and wall losses further reduce the particle concentration. The coagulation also explained the larger particle size (>100 nm, Fig. 1) obtained within the tank compared to those measured by wind tunnel (~50 nm, Table S1) under similar wind speed condition (~30 m s^{-1}), where the particles are homogeneously distributed in a continuous flow and have less chance to coagulate.

In general, the aerosol generated at a wind speed of 25 m s^{-1} was close to that produced under cloud-seeding wind conditions and thus was used for further ice nucleation measurements.

Particles with distinct diameters (D_p) of 90 nm, 200 nm and 400 nm were selected. The 90 nm particles were the smallest selectable and detectable particle size due to the rapid coagulation of particles with smaller sizes. In addition, particles with a diameter of 200 nm and 400 nm were selected which represent the typical size range of the generated accumulation mode aerosol.

3.2 Ice nucleation ability of flare-generated aerosols

The FF of the particles as a function of temperature is shown in Fig. 2. The observed temperature range from 244 K to 267 K is determined by the lowest (~0) and highest FF (~1) detected in our instrument. The INA (represented by FF) of the flare-generated aerosols was found to be size-dependent (Fig. 2a). A progressively lower FF was observed as the particle size decreased. This can also be observed by considering the temperature at which each particle size reaches a $FF \approx 1$. For the 90 nm, $FF \approx 1$ was reached at T ≈ 253 K but for the 200 and 400 nm particles, $FF \approx 1$ was reached at 258 K (Fig. 2a). This is expected because the larger particles have a higher probability of containing an effective ice-active site with increasing surface area. For pure AgI particles, *Marcolli et al.* [2016] reported some dissolution after being immersed in cloud droplets of the same sizes as reported here, which leads to the erosion of the particle surface and reduction of its INA. *Marcolli et al.* [2016] reported the partial dissolution of 0.04% for 200 nm particles but 38% for 20 nm particles which reduced their INA for the latter. In our case, the dissolution for particles is expected to be higher because of the overall low AgI content (~11.8% of the flare mass) within the same size of a cloud droplet. In other words, not the entire particle size of 90, 200 or 400 nm selected here is composed of AgI.

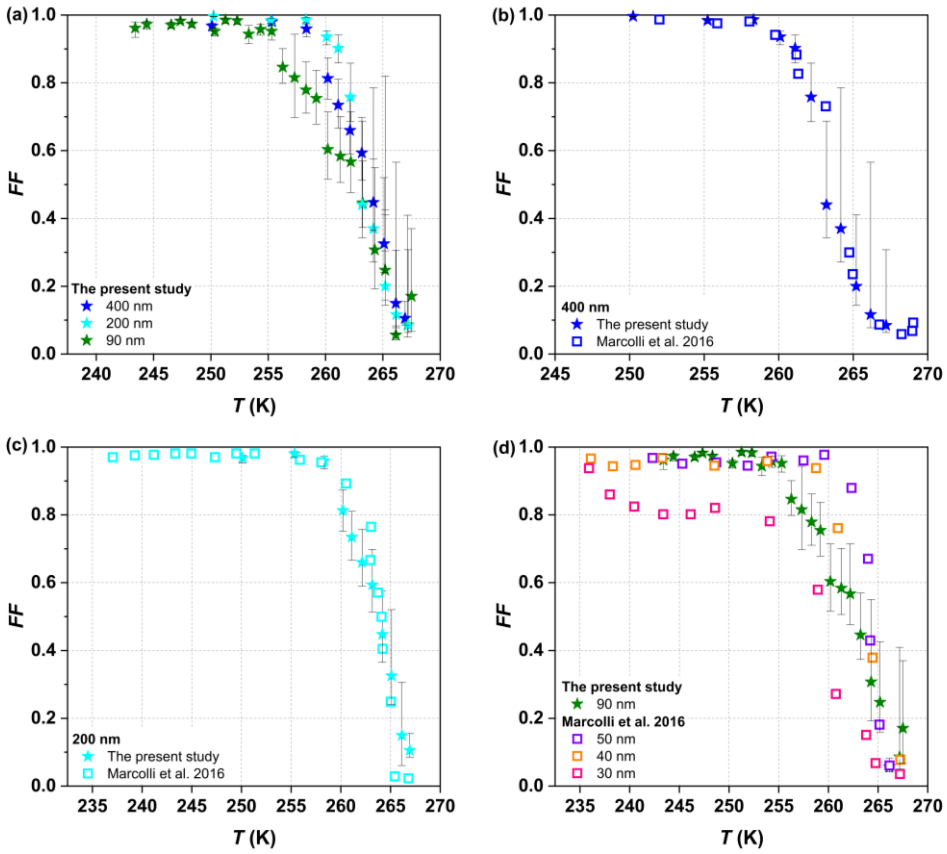

Figure 2. Frozen fraction (FF) as a function of the temperature of flare-generated aerosols from this work (panel a) compared to those of similar sizes from *Marcolli et al.* [2016] (panels b, c

and d). Stars represent flare-generated aerosol which was a mixture of AgI particles and by-products produced (such as ammonium perchlorate, and volatile compounds) and diamond symbols represent the pure AgI particles generated from a AgI-water suspension [*Marcolli et al.*, 2016].

The immersion freezing observed in this work can be compared to those of pure AgI particles generated from a AgI-water suspension [*Marcolli et al.*, 2016] (Figs. 2b-d). Similar to flare particles, the *FF* of pure AgI particles exhibits a size-dependent behavior (Fig. 2d). AgI particles with sizes of 40 nm and 50 nm reach $FF \approx 1$ at 260 K, whereas 30 nm AgI particles reach $FF \approx 1$ at homogeneous freezing temperature (235 K). Therefore, the critical size for AgI particles to nucleate ice efficiently is 40 nm, where the full INA potential ($FF \approx 1$) is reached before homogeneous freezing temperature. The pure AgI and flare particles show excellent agreement in *FF* for the 200 and 400 nm size particles (Figs. 2b-c). The INA of 90 nm flare-generated particles is lower than 40 nm but higher than 30 nm pure AgI particles (Figs. 2d), as the 90 nm flare particles reach $FF \approx 1$ at 253 K versus 260 K and 235 K for the 40 nm and 30 nm AgI particles. The flare-generated particles contain other soluble components to first promote droplet activation before freezing in real-world cloud-seeding operations. In particular, non-AgI components like ammonium perchlorate, and volatile compounds were produced upon burning. These impurities can either form non-AgI particles or condense onto the AgI particle surface such that a 90 nm flare particle has much less AgI mass than a 90 nm pure AgI particle. At certain particle size, the ratio of AgI to non-AgI components would become critical to assessing the INA of flare particles. Our results indicate that the effect of the non-AgI components on the INA of flare particles is minor for larger particles (200 nm and 400 nm, Figs. 2b-c), as their INA is similar to that of pure AgI (40 nm~50 nm) from *Marcolli et al.* [2016] which we use as a reference here. The critical size for flare-generated aerosol to nucleate ice efficiently is 90 nm, which includes sufficient AgI fraction comparable to 40 nm pure AgI particles (Fig. 2d). Flare particles smaller than this size would have reduced INA due to an insufficient AgI content, as evident by the significant decrease in INA observed for 30 nm AgI particles. In general, as long as the AgI content in flare particles is higher than an equivalent 40 nm pure AgI particle (Fig. 2b-c), their full IN potential is reached. We therefore recommend that cloud-seeding operation with aerosol from such burn-in-place flares should prioritize particles ≥ 90 nm. Moreover, effective cloud-seeding materials should contain a minimum AgI mass equivalent to 40 nm AgI particles to achieve the highest possible INA equivalent to pure AgI particles.

DeMott [1995] investigated the INA of aerosols originating from burning AgI–acetone–ammonium iodide–water solutions in a propane flame. An appreciably lower freezing ability was observed for 30 nm and 70 nm particles compared to the 90 nm flare particles in the present study and pure AgI particles (30 ~ 50 nm, [*Marcolli et al.*, 2016]) (Fig. S7). The varied INAs of AgI-containing aerosols among studies, are evidence that the production method will impact the glaciogenic seeding ability of the particles that depend on the size and composition of the materials being used to generate the AgI aerosols. The characteristics of the additives and how they interact with the AgI particles will modify the INA of the generated aerosols. The flares used here have the closest INA to those of pure AgI particles, and thus could be effective for glaciogenic cloud seeding research and applications.

3.3 Critical mass activated fraction (*critical-n_m*) and its atmospheric application

The change in mass for particles of fixed size over time is shown in Fig. 3a. Since the decay in 90 nm particle number concentration occurred rapidly, the particle mass could not be detected. The 90 nm particle mass was calculated by the particle density derived from the measured average mass of 200 nm particles assuming a spherical shape. The averaged particle mass with respect to the particle size is given in Table S2.

The increase in particle mass over time (Fig.3a), confirms that by-products formed during the burning process were able to condense onto the AgI particle surfaces or smaller particles coagulated, but may not have increased the size detectably. The inhomogeneous chemical composition of flare-generated aerosol and its impact on ice nucleation can also be seen in Fig. S8 from the estimated mass active site density of particles (n_m) calculated by Eq. (3) and the surface ice active site density of particles (n_s) calculated by Eq. (4), where different n_m and n_s values were observed for particles of varying sizes. If particles had the same composition as a function of size, their INA should scale with surface area or mass and the normalized n_m or n_s values should fall onto a single curve. A similar observation is also made for illite clay particles in the size range from 100 ~ 800 nm [*Welti et al.*, 2009], where the calculated n_s falls onto a single curve for 200 ~ 800 nm particles, but the 100 nm particles exhibit a lower n_s because of different composition from larger particles.

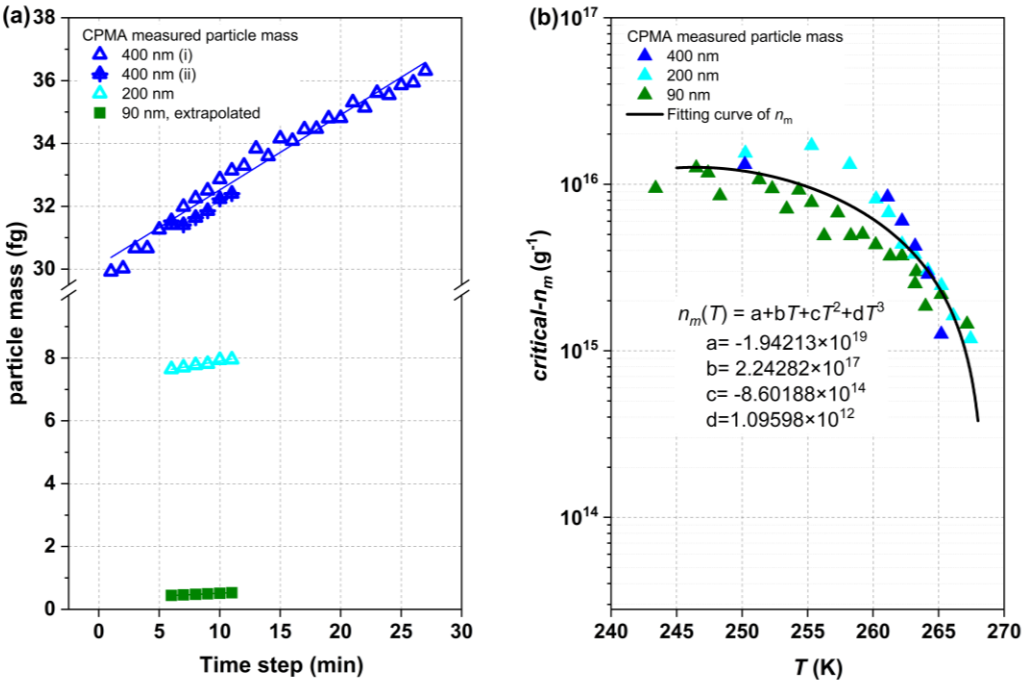

Figure 3. The change in particle mass over time measured by CPMA (a) and the derived critical active site density per unit mass of 40 nm AgI particles (*critical-n_m*) (b). The particle mass of 90 nm particles (a) was calculated based on the 200 nm and 400 nm particles assuming a spherical particle shape and the same particle density. The solid line in (b) shows the parameterization to predict the *critical-n_m*, where a is -1.94213×10^{19}, b is 2.24282×10^{17}, c is -8.60188×10^{14} and d is 1.09598×10^{12}, valid for 245 K <T< 267 K.

From Fig. S8 we can see that 90 nm particles give the highest INA of flare-generated particles is determined by a minimum effective mass of AgI, above which larger seed particles (200 and 400 nm) or more AgI do not increase their INA. The critical size for flare-generated

aerosol to nucleate ice efficiently is 90 nm, as it includes sufficient AgI mass comparable to 40 nm pure AgI particles (Fig. 2d). If n_m was derived based on the total mass of flare-generated particles, the ability of flare to produce INPs would be underestimated. Similarly, if n_m is scaled to particle masses above 40 nm AgI which do not additionally improve the INA, the n_m would also be underestimated. Based on these findings, we derive the critical ice active mass density (*critical-* n_m) from the measured flare particles FF and the critical mass of 40 nm pure AgI particles (0.19 fg, calculated with a AgI particle density of 5.66 g cm^{-3}) required for efficient ice nucleation (Eq. 3). The *critical-*n_m of all considered sizes can be fit by a curve that parameterises the number of ice crystals per gram of seeding material. The new parameterization is displayed in Fig. 3b, with a coefficient of determination (R^2) of 0.72. The substantial coefficient indicates the empirical data obtained aligns well with the values predicted by the proposed parameterization. The parameterization provides the expected ice crystal number concentration produced by the mass of seeding material as a function of seeding temperature, provided each seeding particle contains a minimum of 40 nm AgI. This serves as a reference to optimize the production and efficiency of cloud-seeding materials in practical use. We note that in this work we only report on and support our data on the INA of the flare-generated aerosol, which is the first step for cloud seeding to be successful. The evolution of the seeded cloud, its dynamics and microphysics must be considered and researched further for various desired outcomes.

4 Conclusion

The INA of commercially available cloud-seeding aerosol containing AgI was measured under mixed-phase cloud conditions (243 K <T< 267 K). The aerosol was produced by burn-in-place flares at a high wind speed (25 m s^{-1}) that mimicked the aerosol generation process in real-world aircraft cloud-seeding operations. The generated aerosols have comparable INA to previously reported pure AgI particles in the size range of 200 nm and 400 nm. The non-AgI impurity produced from the same process lowers the INA of particles < 90 nm, where the AgI mass is likely less ≤ 40 nm. Our results imply that if cloud-seeding particle modes of 50-60 nm are produced due to high aircraft windspeeds, these will likely not contain enough AgI mass within them to achieve the full potential of glaciogenic seeding. Favoring larger particle mode sizes ≥90 nm are likely to contain enough AgI mass to reach its full ice seeding potential. For other cloud-seeding materials to reach a good ice nucleation efficiency, it is essential to include a minimum AgI mass equivalent to 40 nm AgI particles. The critical mass ice-activated fraction (*critical-*n_m) of the generated particles was estimated by normalizing the obtained FF with the mass of 40 nm AgI particles. *Critical-*n_m of all considered sizes agree well with each other and its temperature dependence can be described by a new parameterization valid for 245 K–267 K. This parameterization provides the minimum mass of AgI particles needed to produce the said ice crystal density. It holds significant potential in guiding the production and optimization of commercial seeding products.

Acknowledgment

We acknowledge Mr. Frank Kasparek from Cloud Seeding Technologies for providing the commercial ZEUS flare.

Open Research

The data that support the conclusions of this study are available at this site: https://doi.org/10.5281/zenodo.8403462

5 Reference

Cantrell, W., and A. Heymsfield (2005), Production of Ice in Tropospheric Clouds: A Review, *Bulletin of the American Meteorological Society*, *86*(6), 795-808.

Davis, B. L., L. R. Johnson, and F. J. Moeng (1975), An Explanation for the Unusual Nucleating Ability of Aerosols Produced from the AgI-NH4I-Acetone System, *Journal of Applied Meteorology and Climatology*, *14*(5), 891-896.

DeMott, P. J. (1995), Quantitative descriptions of ice formation mechanisms of silver iodide-type aerosols, *Atmospheric Research*, *38*(1), 63-99.

DeMott, P. J., W. G. Finnegan, and L. O. Grant (1983), An Application of Chemical Kinetic Theory and Methodology to Characterize the Ice Nucleating Properties of Aerosols Used for Weather Modification, *Journal of Climate and Applied Meteorology*, *22*(7), 1190-1203.

Dessens, J., J. L. Sánchez, C. Berthet, L. Hermida, and A. Merino (2016), Hail prevention by ground-based silver iodide generators: Results of historical and modern field projects, *Atmospheric Research*, *170*, 98-111.

Edwards, G. R., L. F. Evans, and V. K. La Mer (1962), Ice nucleation by monodisperse silver iodide particles, *Journal of Colloid Science*, *17*(8), 749-758.

Fletcher, N. H. (1970), *The Chemical Physics of Ice*, Cambridge University Press, Cambridge.

French, J. R., K. Friedrich, S. A. Tessendorf, R. M. Rauber, B. Geerts, R. M. Rasmussen, L. Xue, M. L. Kunkel, and D. R. Blestrud (2018), Precipitation formation from orographic cloud seeding, *Proceedings of the National Academy of Sciences*, *115*(6), 1168-1173.

Friedrich, K., et al. (2020), Quantifying snowfall from orographic cloud seeding, *Proceedings of the National Academy of Sciences*, *117*(10), 5190-5195.

Hiranuma, N., et al. (2015), A comprehensive laboratory study on the immersion freezing behavior of illite NX particles: a comparison of 17 ice nucleation measurement techniques, *Atmos. Chem. Phys.*, *15*(5), 2489-2518.

Kanji, Z. A., A. Welti, C. Chou, O. Stetzer, and U. Lohmann (2013), Laboratory studies of immersion and deposition mode ice nucleation of ozone aged mineral dust particles, *Atmos. Chem. Phys.*, *13*(17), 9097-9118.

Kanji, Z. A., L. A. Ladino, H. Wex, Y. Boose, M. Burkert-Kohn, D. J. Cziczo, and M. Krämer (2017), Overview of Ice Nucleating Particles, *Meteorological Monographs*, *58*, 1.1-1.33.

Kerr, R. A. (1982), Cloud Seeding: One Success in 35 Years, *Science*, *217*(4559), 519-521.

Koop, T., B. Luo, A. Tsias, and T. Peter (2000), Water activity as the determinant for homogeneous ice nucleation in aqueous solutions, *Nature*, *406*(6796), 611-614.

Lamb, D. (2003), CLOUD MICROPHYSICS, in *Encyclopedia of Atmospheric Sciences*, edited by J. R. Holton, pp. 459-467, Academic Press, Oxford.

Lohmann, U., F. Lüönd, and F. Mahrt (2016), *An Introduction to Clouds: From the Microscale to Climate*, Cambridge University Press, Cambridge.

Lüönd, F., O. Stetzer, A. Welti, and U. Lohmann (2010), Experimental study on the ice nucleation ability of size-selected kaolinite particles in the immersion mode, *Journal of Geophysical Research: Atmospheres*, *115*(D14).

Manton, M. J., and L. Warren (2011), A Confirmatory Snowfall Enhancement Project in the Snowy Mountains of Australia. Part II: Primary and Associated Analyses, *Journal of Applied Meteorology and Climatology*, *50*(7), 1448-1458.

Marcolli, C., B. Nagare, A. Welti, and U. Lohmann (2016), Ice nucleation efficiency of AgI: review and new insights, *Atmos. Chem. Phys.*, *16*(14), 8915-8937.

Murray, B. J., D. O'Sullivan, J. D. Atkinson, and M. E. Webb (2012), Ice nucleation by particles immersed in supercooled cloud droplets, *Chem. Soc. Rev.*, *41*(19), 6519-6554.

Nagare, B., C. Marcolli, A. Welti, O. Stetzer, and U. Lohmann (2016), Comparing contact and immersion freezing from continuous flow diffusion chambers, *Atmos. Chem. Phys.*, *16*(14), 8899-8914.

Nicolet, M., O. Stetzer, F. Lüönd, O. Möhler, and U. Lohmann (2010), Single ice crystal measurements during nucleation experiments with the depolarization detector IODE, *Atmos. Chem. Phys.*, *10*(2), 313-325.

Palanisamy, M., K. Thangaraj, R. Gobinathan, and P. Ramasamy (1986), X-ray diffraction and ice nucleation studies of AgI AgCl solid solutions, *Journal of Crystal Growth*, *79*(1, Part 2), 1005-1009.

Pokharel, B., and B. Geerts (2016), A multi-sensor study of the impact of ground-based glaciogenic seeding on clouds and precipitation over mountains in Wyoming. Part I: Project description, *Atmospheric Research*, *182*, 269-281.

Pokharel, B., B. Geerts, X. Jing, K. Friedrich, K. Ikeda, and R. Rasmussen (2017), A multi-sensor study of the impact of ground-based glaciogenic seeding on clouds and precipitation over mountains in Wyoming. Part II: Seeding impact analysis, *Atmospheric Research*, *183*, 42-57.

Rauber, R. M., B. Geerts, L. Xue, J. French, K. Friedrich, R. M. Rasmussen, S. A. Tessendorf, D. R. Blestrud, M. L. Kunkel, and S. Parkinson (2019), Wintertime Orographic Cloud Seeding—A Review, *Journal of Applied Meteorology and Climatology*, *58*(10), 2117-2140.

Shevkunov, S. V. (2005), Computer Simulation of the Initial Stage of Water Vapor Nucleation on a Silver Iodide Crystal Surface: 1. Microstructure, *Colloid Journal*, *67*(4), 497-508.

Shevkunov, S. V. (2008), Stimulation of vapor nucleation on perfect and imperfect hexagonal lattice surfaces, *Journal of Experimental and Theoretical Physics*, *107*(6), 965-983.

Silverman, B. A. (2010), An evaluation of eleven operational cloud seeding programs in the watersheds of the Sierra Nevada Mountains, *Atmospheric Research*, *97*(4), 526-539.

Stetzer, O., B. Baschek, F. Lüönd, and U. Lohmann (2008), The Zurich Ice Nucleation Chamber (ZINC)-A New Instrument to Investigate Atmospheric Ice Formation, *Aerosol Science and Technology*, *42*(1), 64-74.

Vonnegut, B. (1947), The Nucleation of Ice Formation by Silver Iodide, *Journal of Applied Physics*, *18*(7), 593-595.

Vonnegut, B. (1949), Nucleation of Supercooled Water Clouds by Silver Iodide Smokes, *Chemical Reviews*, *44*(2), 277-289.

Welti, A., U. Lohmann, and Z. A. Kanji (2019), Ice nucleation properties of K-feldspar polymorphs and plagioclase feldspars, *Atmos. Chem. Phys.*, *19*(16), 10901-10918.

Welti, A., F. Lüönd, O. Stetzer, and U. Lohmann (2009), Influence of particle size on the ice nucleating ability of mineral dusts, *Atmos. Chem. Phys.*, *9*(18), 6705-6715.

Welti, A., F. Lüönd, Z. A. Kanji, O. Stetzer, and U. Lohmann (2012), Time dependence of immersion freezing: an experimental study on size selected kaolinite particles, *Atmos. Chem. Phys.*, *12*(20), 9893-9907.